Rare Metal Materials and Engineering
Volume 51, Issue 3, March 2022
Available online at www.rmme.ac.cn

Science Press

Cite this article as: Fu Tianlin, Mei Changyun, Chen Feifan, et al. Influence of Surface Nanocrystallization on Microstructure and Properties of Anodic Oxide Film on Pure Titanium[J]. Rare Metal Materials and Engineering, 2022, 51(03): 835-842.

ARTICLE

Influence of Surface Nanocrystallization on Microstructure and Properties of Anodic Oxide Film on Pure Titanium

Fu Tianlin[1,2], Mei Changyun[1], Chen Feifan[1], Xu Zhihua[1]

[1] Research Institute of Small Domestic Appliance Division, Midea Group, Foshan 528000, China; [2] School of Materials Science and Engineering, South China University of Technology, Guangzhou 510641, China

Abstract: The surface gradient nanocrystalline structure was fabricated by the surface mechanical attrition treatment (SMAT), and the influence of surface nanocrystallization on the surface microstructure and characteristic of passive film on pure titanium was studied. The anodic oxidation was conducted in 0.5 mol/L H_2SO_4 solution under the potentiostatic mode at 30 V for different durations to investigate the surface characteristic and corrosion resistance of the passive films by optical microscope, X-ray diffraction, Raman spectrometer, X-ray photoelectron spectroscopy, and electrochemical test. The results show that the gradient nanocrystalline structure can increase the film thickness, promote the crystallization, and improve the corrosion resistance of passive film. The influence mechanism of surface nanocrystallization on the corrosion resistance can be explained by the cation-anion-vacancy condensation.

Key words: surface mechanical attrition treatment; gradient nanocrystalline structure; titanium; anodic oxidation; ceramic layer; corrosion resistance

Titanium alloys are widely used in aerospace, biological engineering, chemical engineering, and marine engineering due to their good biocompatibility, high specific strength, and excellent corrosion resistance[1] caused by the stable native oxide film[2,3]. However, the native oxide film has an amorphous structure with the thickness of 4~6 nm[4], which leads to inferior mechanical properties and potential damage at low sheer stress[5,6]. Furthermore, the native oxide film contains multivalent Ti[7] which is less thermodynamically stable than Ti^{4+} and can be destroyed easily under severe corrosion environment, resulting in the crevice corrosion[8].

Various surface modification methods have been used to enhance the corrosion resistance and wear resistance of titanium alloys[9,10]. The anodic oxidation is an important treatment method due to its low cost and easy operation[11]. In general, the growth and crystallization of anodic titanium oxide films can be promoted by raising the applied voltage[12], prolonging the anodizing time[13], or enhancing the solution temperature[14]. However, it is found that the anodic oxide film prepared by anodic oxidation treatment is partially crystallized and has lots of "flower-like" or "nodule-like" structures on the surface[15].

The substrates also have great influence on the formation and crystallizing process of passive film on titanium alloys. Capek et al[16] found that the anodic oxide films formed on the polished titanium surface are smoother and more compact than those on unpolished titanium substrates. The surface mechanical attrition treatment (SMAT) is an effective way to fabricate surface nanocrystallization on metallic materials. Tong et al[17] found that SMAT can reduce the nitriding temperature of Fe. Lei et al[18] fabricated a ceramic coating of 10 μm in thickness by micro arc oxidation (MAO) process after SMAT on 2024 Al alloy, and found that SMAT-MAO treatment has a positive influence on corrosion resistance of films. Ou et al[19] fabricated the superhydrophobic film on NiTi alloy surface by SMAT and anodization, and found that SMAT increases the thickness of the passive film and improves the wetting uniformity of the NiTi surface.

In this research, the pure titanium was selected as the substrate. The influence of surface nanocrystallization on the passive films on pure titanium was investigated. The crystallization process, film thickness, chemical composition, corrosion resistance, and the breakdown process of passive films were discussed.

Received date: March 19, 2021
Corresponding author: Chen Feifan, Ph. D., Research Institute of Small Domestic Appliance Division, Midea Group, Foshan 528000, P. R. China, E-mail: feifan1.chen@midea.com

1 Experiment

The chemical composition of the pure titanium (TA2) is listed in Table 1. During SMAT, the specimen surface was strongly impacted in a short time using a high frequency system (50 kHz). Then the TA2 and SMATed TA2 specimens were cut into the size of 50 mm×10 mm×1 mm, and cleaned with acetone, alcohol, and deionized water under ultrasonic condition. The anodic oxidation was conducted in a two-electrode electrochemical cell. Each specimen was used as the anode and the graphite plate was used as the cathode. The anode and cathode were positioned face-to-face with 10 mm in distance. During the anodic oxidation treatment in 0.5 mol/L H_2SO_4 solution, the potential was kept at 30 V for 3600 s. The TA2 and SMATed TA2 specimens after the final anodic oxidation were named as O-Ti_{30} and SMAT-Ti_{30} specimens, respectively.

The surface morphology was observed using scanning electron microscopy (SEM, LEO 1530Vp, Carl Zeiss AG, Germany) at an acceleration voltage of 15 kV. A Raman spectrometer (LabRAM HR Evolution, Horiba Group, Japan) equipped with an optical microscope (OM) was used to detect the crystallization of anodic oxide films with the excitation wavelength of 532 nm and the incident power of 10.4 mW. For the thickness measurement of anodic oxide films, X-ray photoelectron spectroscope (XPS, PHI5000 Versaprobe-II, Shimadzu Co., Ltd, Japan) analysis was performed using Al-Kα radiation. The surface was sputtered over an area of 4 mm×4 mm using the Ar^+ ion beam of 3000 eV.

The corrosion resistance was evaluated via the electrochemical test on the electrochemical workstation (CHI 760E, Shanghai Chenghua Instrument Co., Ltd, China) in 10wt% NaCl solution at 70 °C. A saturated calomel electrode (SCE) was used as the reference electrode, a platinum coil was used as the counter electrode, and the specimens were used as the working electrodes. The potentiodynamic polarization tests were initiated after immersion of the specimens for 1 h until a stable open circuit potential was obtained, and the scanning rate was 3 mV/s from −3000 mV to 4000 mV. The corrosion potential (E_{corr}) and corrosion current density (j_{corr}) were determined from the polarization curves by the Tafel extrapolation method. The anodic oxide films on the O-Ti_{30} and SMAT-Ti_{30} specimens were characterized via the Mott-Schottky analysis, during which the potential was scanned along the anode-to-cathode direction at a scanning interval of 50 mV. The alternating current (AC) signal with a frequency of 1000 Hz and a peak-to-peak magnitude of 10 mV was superimposed on the scanning potential, and the capacitance was measured at each applied potential.

Table 1 Chemical composition of TA2 (wt%)

C	Fe	O	N	H	Ti
0.02	0.10	0.15	0.02	0.0011	Bal.

2 Results and Discussion

2.1 Surface microstructure

Fig.1 shows OM images of original TA2 (Fig.1a) and cross-section microstructure of SMATed TA2 specimens (Fig. 1b). Before processing, the TA2 specimen was annealed in vacuum at 873 K for 6 h. The microstructure of TA2 shows an equiaxed microstructure with the average grain size of 50 μm. During SMAT process, the severe plastic deformation region is formed in the surface, and there is no sharp interface between the deformation zone and the matrix. The deformation layer consists of two parts: the severely deformed surface layer of 100 μm in thickness and the subsurface layer with many deformation bands and twins. The closer the subsurface layer to the surface layer, the denser the microstructure.

Because TA2 specimen has a small amount of active slip at room temperature, the twinning plays an important role in deformation under dynamic loading[20]. The similar phenomena can also be observed in the near-α titanium alloy[21] and α-titanium[22] after severe plastic deformation treatment.

Fig. 1c shows XRD patterns of the original TA2 and SMATed TA2 specimens, indicating that the full width at half maximum (FWHM) of the diffraction peaks of SMATed TA2 specimen is larger than that of the original TA2 specimen, because of the grain refinement and the increasing micro-strain at atomic-level[23]. The average crystallite size of SMATed TA2 specimens is about 35 nm, according to the calculation based on FWHM of Bragg diffraction peaks of (002), (101), (102), and (103) planes via Scherrer-Wilson equation[18]. The Scherrer-Wilson equation is as follows[24]:

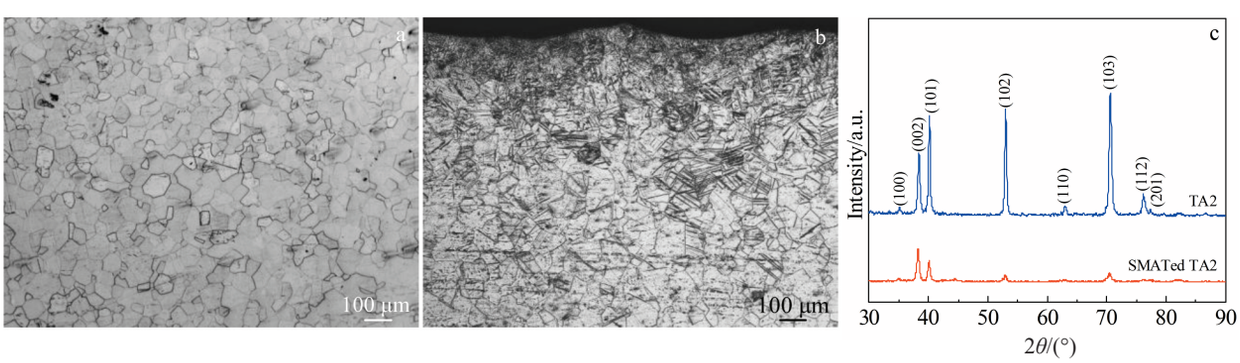

Fig.1 OM images of TA2 (a) and cross-sectional SMATed TA2 (b) specimens; XRD patterns of TA2 and SMATed TA2 specimens (c)

$$D=k\lambda/\beta\cos\theta \quad (1)$$

where λ is the X-ray wavelength, β is the FWHM of diffraction peak, θ is the Bragg angle, D is the average crystallite size, and the constant $k\approx1$. This result demonstrates that the grain size decreases to nano-scale through SMAT.

2.2 Chemical composition of anodic oxide films

As shown in Fig. 2, the wide-range XPS spectra of the O-Ti_{30} and SMAT-Ti_{30} specimens have the peaks of Ti 2p, O 1s, and C 1s. Fig.3 shows the variation of atomic percentages of O and Ti with sputtering depth in the passive films formed on different specimens. Vesel et al[25] found that the depth where the oxygen content is 50% of its maximum value indicates the thickness of the passive film. As shown in Fig.3, the thickness of the passive film of O-Ti_{30} and SMAT-Ti_{30} specimens is about 114 and 1160 nm, respectively.

Fig.4 and Fig.5 show the high-resolution XPS spectra of Ti $2p_{3/2}$ and O 1s at different depths of the passive films of O-Ti_{30} and SMAT-Ti_{30} specimens, respectively. It can be inferred that the Ti, Ti^{2+}, Ti^{3+}, Ti^{4+}, O^{2-}, OH^-, and H_2O may exist in the passive films according to the chemical state of Ti and O elements, as shown in Table 2[26,27].

After deconvolution by Gaussian-Lorentzian functions, the Ti $2p_{3/2}$ narrow-scan spectra reveal a major peak at 458.01 eV corresponding to Ti^{4+}, as shown in Fig. 4a. The O 1s narrow-scan spectra (Fig. 4b) consist of three peaks corresponding to O^{2-}, OH^-, and adsorbed water. The O^{2-} may originate from TiO_2, and the OH^- and the adsorbed water may come from the hydrated titanium oxides[6]. These peaks suggest that the passive film surface of O-Ti_{30} specimen consists of TiO_2, $Ti(OH)_4$, and $TiO_2\cdot nH_2O$. The Ti 2p spectra at the depth of 52 nm result from the Ti^{4+} and Ti^{2+}, and the O 1s spectra at the depth of 52 nm result from O^{2-} and OH^-. XPS analysis indicates that the anodic oxide film mainly consists of TiO_2, TiO, and $Ti(OH)_4$ in the depth range of 0~52 nm. At the depth of 75 nm, the Ti^{4+} peaks weaken whereas the Ti^{2+} peaks increase. In the depth from 75 nm to 143 nm, the anodic oxide film is a mixture of Ti_2O_3, TiO, and metallic Ti. At the depth of 196 nm, both Ti_2O_3 and TiO disappear and only the metallic Ti can be observed.

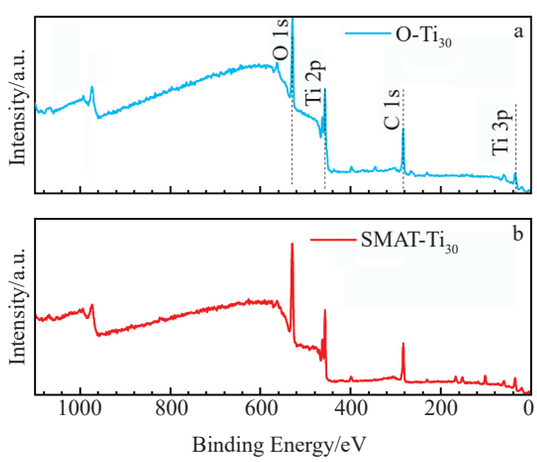

Fig.2 XPS spectra of anodic oxide films of O-Ti_{30} (a) and SMAT-Ti_{30} (b) specimens

As shown in Fig. 5, the Ti element mainly appears in the forms of TiO_2, $Ti(OH)_4$, and $TiO_2\cdot nH_2O$ in the outmost surface (0 nm). In the depth from 0 nm to 252 nm, the components in the oxide film are a mixture of TiO_2, TiO, and $Ti(OH)_4$. In the depth range of 252~508 nm, the components in the oxide film are a mixture of TiO_2 and $Ti(OH)_4$ with a small amount of metallic Ti. In the depth of 508~1010 nm, the components mainly consist of TiO_2, Ti_2O_3, and metallic Ti. At the depth of 1252 nm, both Ti-oxide and Ti-hydroxide disappear and only the metallic Ti can be observed.

The main components of anodic oxide film of both O-Ti_{30} and SMAT-Ti_{30} specimens are oxides at high valence and hydroxide at the outer part of oxide film, and metallic Ti and oxides at low valence at the inner part of oxide film. The nanocrystalline surface prepared by SMAT greatly increases the thickness of the oxide film from 114 nm to 1160 nm, and the range of oxides at high valence also increases. During the anodic oxidation, the lattice diffusion is not significant owing to its considerably small temperature coefficient, and the grain boundary diffusion plays a significant role[5]. Due to the numerous grain boundaries in the severe plastic deformation region, the adsorption and diffusion of oxygen are faster for the SMATed TA2 specimen than the original TA2 specimen.

2.3 Crystallization

The OM images and Raman spectra of the passive films of O-Ti_{30} and SMAT-Ti_{30} specimens are shown in Fig. 6. The anodized film on original TA2 (Fig. 6a) has two different

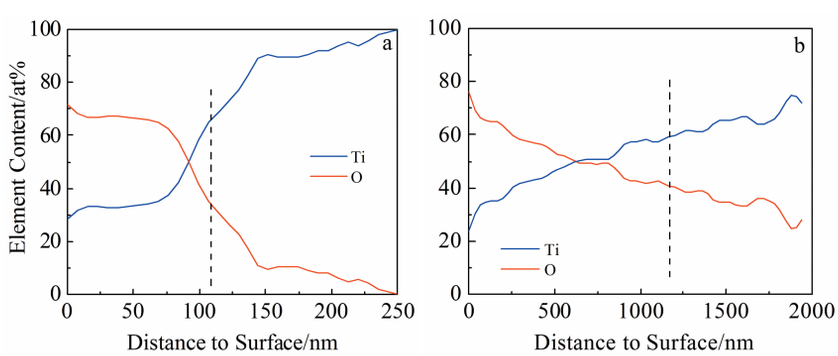

Fig.3 Relationship between element contents and sputtering depth in anodic oxide films of O-Ti_{30} (a) and SMAT-Ti_{30} (b) specimens

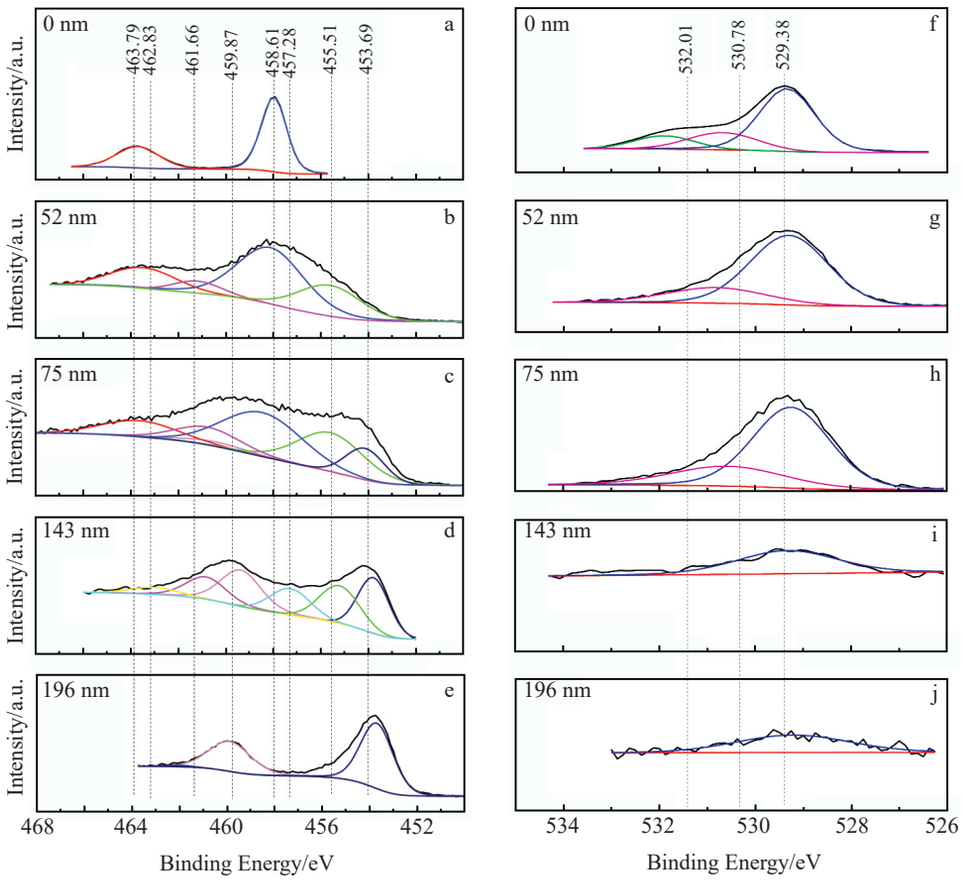

Fig.4 High-resolution XPS spectra of Ti $2p_{3/2}$ (a~e) and O 1s (f~j) at different depths of passive oxide films of O-Ti_{30} specimens: (a, f) 0 nm, (b, g) 52 nm, (c, h) 75 nm, (d, i) 143 nm, and (e, j) 196 nm

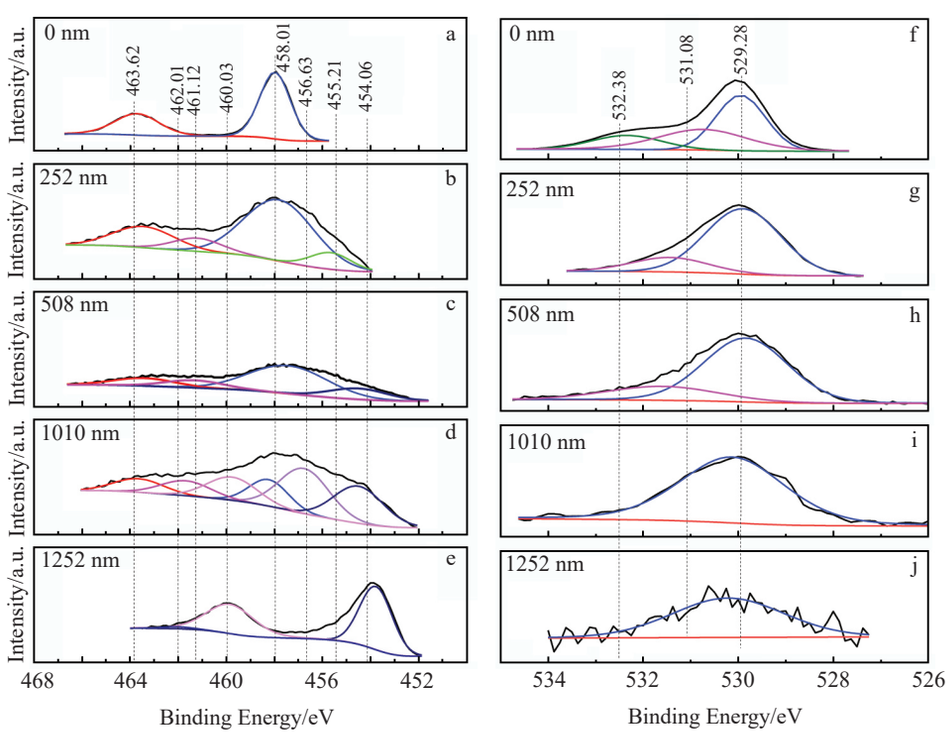

Fig.5 High-resolution XPS spectra of Ti $2p_{3/2}$ (a~e) and O 1s (f~j) at different depths of passive oxide films of SMAT-Ti_{30} specimens: (a, f) 0 nm, (b, g) 252 nm, (c, h) 508 nm, (d, i) 1010 nm, and (e, j) 1252 nm

Table 2 Standard energies of different XPS peaks (eV)[26,27]

Ti $2p_{3/2}$				O 1s		
Ti	Ti^{2+}	Ti^{3+}	Ti^{4+}	O^{2-}	OH^-	H_2O
453.6	455.9	457.3	530.2	530.2	532.5	533.4

regions: a bright region and a dark region, indicating that the crystallization behavior of the anodized film is not uniform. On the contrary, the microstructure of SMAT-Ti_{30} specimen shows a relatively homogeneous feature (Fig.6b), indicating a relatively uniform crystallization.

In Fig.6c, the Raman spectra consist of four peaks at around 144, 405, 516, and 639 cm^{-1}, which are related to the long-range order and short-range order of anatase phase[28]. In detail, the Raman band at around 144 cm^{-1} indicates the long-range order of anatase phase, and Raman bands at about 405, 516, and 639 cm^{-1} indicate the short-range order of anatase phase[29]. When the Raman micro-laser beam is focused on the dark region of the passive film of O-Ti_{30} specimen, a weak peak can be observed at around 144 cm^{-1}. However, there is no peak when the beam is centered on the light region.

Xing et al[13] suggested that the intensity of Raman bands is directly proportional to the crystallinity of the passive film. Therefore, the peak intensity of SMAT-T_{30} specimen is generally stronger than that of O-Ti_{30} specimen, indicating that the crystallization of passive films is promoted by the surface nanocrystallization.

2.4 Electrochemical tests

The potentiodynamic polarization curves of O-Ti_{30} and SMAT-Ti_{30} specimens in 10wt% NaCl solution at 70 °C are shown in Fig. 7a. The anodic part of the polarization curves indicates that both the O-Ti_{30} and SMAT-Ti_{30} specimens show the passivation characteristics. In the passive region of the SMAT-Ti_{30} specimen, the current density barely changes. However, the current density of the O-Ti_{30} specimen is increased with increasing the applied corrosion potential, which may be attributed to the dissolution of the oxide film in 10wt% NaCl solution at 70 °C.

Based on the potentiodynamic polarization curves, the corrosion potential E_{corr} and corrosion current density j_{corr} can be obtained. The j_{corr} can be obtained by extrapolating the cathodic Tafel line to the E_{corr} point[30,31]. Thus, the value of E_{corr} is −1.12 and −0.68 V vs. SCE and corresponding j_{corr} is 5.01×10^{-5} and 1.25×10^{-5} A·cm^{-2} for the O-Ti_{30} and SMAT-Ti_{30} specimens, respectively. The SMAT-T_{30} specimen has higher E_{corr} and lower j_{corr}, compared with the O-Ti_{30} specimen, which indicates the less tendency to corrosion and slower corrosion rate. Thus, the SMAT-Ti_{30} specimen exhibits a better corrosion resistance[32].

It is well known that a relationship exists between the semiconducting properties and corrosion resistance of an anodic oxide film. These properties can be determined by the Mott-Schottky plot with capacitance as a function of electrode

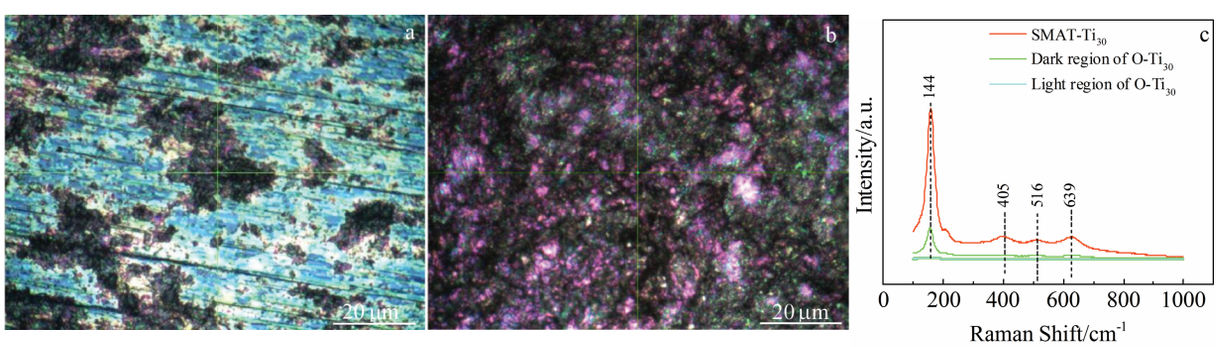

Fig.6 OM images of passive films of O-Ti_{30} (a) and SMAT-Ti_{30} (b) specimens; Raman spectra of anodic oxide films of O-Ti_{30} and SMAT-Ti_{30} specimens (c)

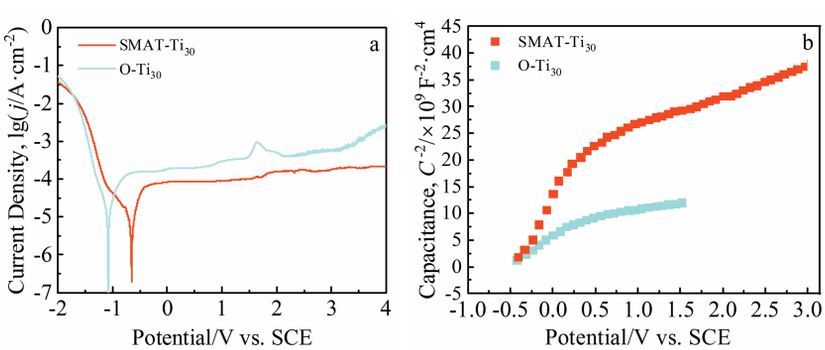

Fig.7 Potentiodynamic polarization curves (a) and Mott-Schottky plots (b) of O-Ti_{30} and SMAT-Ti_{30} specimens in 10wt% NaCl solution at 70 °C

potential, which reflects the charge distribution in the passive film. According to Mott-Schottky analysis, two capacitances should be considered: the capacitance of space charge layer and the capacitance of Helmholtz layer[33]. These capacitances are in series and the total capacitance C is expressed as follows:

$$\frac{1}{C^2}=\frac{1}{C_{SC}^2}+\frac{1}{C_H^2} \quad (2)$$

where C_{SC} is the capacitance of the space charge layer and C_H is the capacitance of the Helmholtz layer. Under high frequency (>1 kHz), the capacitance of space charge layer is significantly smaller than that of Helmholtz layer. Therefore, the contribution of the capacitance of Helmholtz layer to the total capacitance can be neglected, and the capacitance of space charge layer can be considered as the total capacitance[34]. The charge distribution at the semiconductor/electrolyte interface can be typically determined from the Mott-Schottky relations which describe the dependence of C_{SC} on electrode potential E[35], as follows:

$$\frac{1}{C_{SC}^2}=\frac{2}{\varepsilon\varepsilon_0 eN_A}\left(E-E_{fb}-\frac{kT}{e}\right) \text{ for n-type semiconductor} \quad (3)$$

$$\frac{1}{C_{SC}^2}=-\frac{2}{\varepsilon\varepsilon_0 eN_D}\left(E-E_{fb}-\frac{kT}{e}\right) \text{ for p-type semiconductor} \quad (4)$$

where E is the applied potential; E_{fb} is the flat band potential; ε_0 is the permittivity of free space; ε is the relative dielectric constant; N_A is the donor density for n-type semiconductors; N_D is the acceptor density for p-type semiconductors; k is the Boltzmann constant; T is the absolute temperature; e is the charge of the electron. N_D/N_A and E_{fb} can be determined from the slope of the experimentally obtained $1/C^2$-E plots and extrapolation result of the linear portion to $1/C^2=0$, respectively. The shape of the Mott-Schottky plot can infer the conductivity type of the semiconductor, i.e., the negative and positive slopes correspond to the p-type and n-type semiconductors, respectively. Furthermore, the concentration of free charge carriers can be determined by the slope of the $1/C_{SC}^2$-E plot; E_{fb} can be determined by the intercept with the potential axis ($1/C_{SC}^2=0$) of the $1/C_{SC}^2$-E plot[36].

In order to understand the semiconductive properties of the anodic oxide films of O-Ti_{30} and SMAT-Ti_{30} specimens, Fig.7b shows the Mott-Schottky plots of specimens passivated under the open circuit potential. A significantly lower donor density N_D (3.5×10^{19} cm^{-3}) can be obtained for the SMAT-Ti_{30} specimen, compared with that of the O-Ti_{30} specimen (5.6×10^{21} cm^{-3}). Since N_D represents the affinity of aggressive anions to the anodic oxide film, the O-Ti_{30} specimens with higher N_D present a larger sensitivity to corrosion with an easier incorporation of aggressive anions to the anodic oxide film. This result is coincident with the lower breakdown potential in the potentiodynamic curves for O-Ti_{30} specimens.

Point defects transfer the electrical current through the anodic oxide film and then the defect reactions occur at the metal|film (M|f) and film|solution (f|s) interfaces, which ultimately causes the breakdown of the anodic oxide film[37]. The schematic diagram of point defect model (PDM) and related reactions used to describe the breakdown process of oxide films on Ti surface is shown in Fig.8.

The equations are expressed in Kröger-Vink notation[38], where the subscripts O and Ti denote the structural oxygen site and titanium site, respectively; the superscript "$\cdot$" or "$'$" denotes one positive or one negative charge, respectively; V represents a vacancy. The electrolyte solution consists of Ti^{4+}(aq) hydrated metal cations.

According to PDM[39], the defects are generated and disappear at the Ti|f and f|s interfaces. The reactions $Ti+V_{Ti}''''\rightarrow Ti_{Ti}$ and $Ti\rightarrow Ti_{Ti}+2V_O^{\cdot\cdot}$ occur at the Ti|f interface, which expresses the submergence of cation vacancies (V_{Ti}'''') into the Ti lattice and the generation of anion vacancies, respectively. The Ti_{Ti} is formed in the oxide lattice and a vacancy V_{Ti}'''' is generated in the Ti lattice. Then the atom Ti reacts with V_{Ti}'''' in the Ti lattice to generate oxygen vacancies ($V_O^{\cdot\cdot}$) and Ti_{Ti} in the oxide lattice.

The reactions $Ti_{Ti}+(V_{Ti}''''V_O^{\cdot\cdot})''\rightarrow V_{Ti}''''+(Ti_{Ti}2V_O^{\cdot\cdot})$ and $O_O\leftarrow V_O^{\cdot\cdot}+H_2O\rightarrow 2H_{aq}^+$ occur at the f|s interface. The former reaction leads to the formation of cation vacancy V_{Ti}'''' and hydrated titanium complex $Ti(H_2O)_n^{4+}$. Then the $Ti(H_2O)_n^{4+}$ ions leave the oxide and therefore metal cations Ti_{Ti} from the oxide lattice are transferred into the solution. The latter reaction indicates the absorption of O^{2-} from H_2O into $V_O^{\cdot\cdot}$, resulting in the oxygen ions O_O into the oxide lattice. When the specimen is immersed in the solution, there was a potential difference due to the difference between the metal phase and the solution phase. The potential difference is distributed across the interphases of M|f ($\phi_{M|f}$) and f|s ($\phi_{f|s}$)[38]. $V_O^{\cdot\cdot}$ and V_{Ti}'''' are diffused through the oxide film by electric field and concentration gradient. The O_O ions are transferred through $V_O^{\cdot\cdot}$ towards the Ti|f and f|s interfaces simultaneously. V_{Ti}'''' is transferred towards the Ti|f interface and it disappears at the Ti side. The cation-vacancy disappearance leads to $V_O^{\cdot\cdot}/V_{Ti}''''$ interactions, which are driven by the electrostatic attraction between opposite-charged defects of high contents[40].

During the reaction of $Cl^-\cdot nH_2O\rightarrow nH_2O+Cl^-$, Cl^- is formed

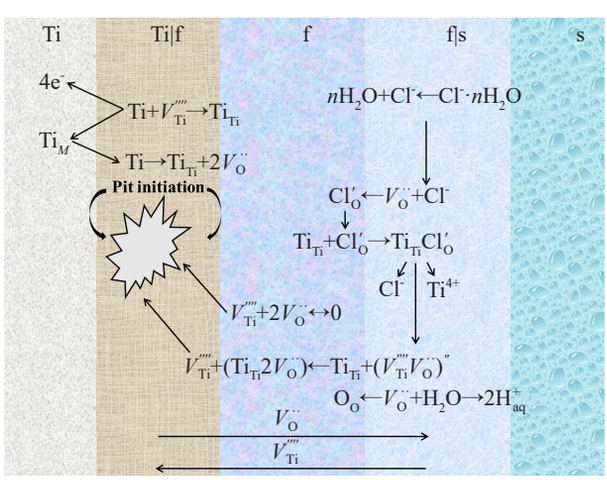

Fig.8 Schematic diagram of breakdown process of anodic oxide film based on point defect model

via the diffusion and migration of Cl^- through the f|s interface. Some Cl^- anions may be absorbed by oxygen vacancies, leading to the formation of Cl defects ($Cl_O^{\cdot}$) which reacts with Ti_{Ti}, thereby resulting in the generation of $Ti_{Ti}Cl_O^{\cdot}$. Subsequently, $Ti_{Ti}Cl_O^{\cdot}$ extraction occurs at f|s interface, resulting in the generation of Cl^-, Ti^{4+}, and a cation vacancy/oxygen vacancy pair ($V_O^{\cdot\cdot}V_{Ti}^{''''}$), which corresponds to the passive film dissolution. Moreover, the reaction between Cl^- and $V_O^{\cdot\cdot}$ reduces the concentration of $V_O^{\cdot\cdot}$, which further leads to the accumulation of $V_{Ti}^{''''}$.

As the excess $V_{Ti}^{''''}$ is accumulated at the Ti|f interface, the $V_{Ti}^{''''}$ condensate is formed, resulting in the separation of the oxide layer from the metal substrate. The breakdown may occur when the average areal concentration of vacancies exceeds the critical value (7.17×10^{15} cm^{-2})[41]. Therefore, N_D is increased with increasing the affinity of Cl^-. In general, SMAT reduces the donor density of the surface layer, and therefore SMAT-Ti_{30} specimen possesses better corrosion resistance. The breakdown of the oxide film is dominated by the cation-anion-vacancy condensation mechanism.

3 Conclusions

1) The surface nanocrystallization has a positive effect on the crystallization of the anodic oxide film, which also increases the thickness of the anodic oxide film. The higher corrosion potential and smaller corrosion current density can be achieved with increasing the anodic potential, therefore obtaining the passive film with better corrosion resistance. A significantly smaller donor density for n-type semiconductors of 3.5×10^{19} cm^{-3} is achieved for the Ti alloys after surface nanocrystallization with passive film.

2) The surface mechanical attrition treatment can reduce the donor density of the anodic oxide film.

3) The breakdown of the oxide film is dominated by the cation-anion-vacancy condensation mechanism.

References

1 Diamanti M V, Pedeferri M P. *Corrosion Science*[J], 2007, 49(2): 939

2 Oliveira V M C A, Aguiar C, Vazquez A M *et al*. *Corrosion Science*[J], 2014, 88(4): 317

3 Jiang Z, Xin D, Norby T *et al*. *Corrosion Science*[J], 2011, 53(2): 815

4 Li S M, Yao W H, Liu J H *et al*. *Surface and Coatings Technology*[J], 2015, 277: 234

5 Wen M, Wen C, Hodgson P *et al*. *Corrosion Science*[J], 2012, 59: 352

6 Park Y J, Song H J, Kim I *et al*. *Journal of Materials Science: Materials in Medicine*[J], 2007, 18(4): 565

7 Hanawa T. *Materials Science & Engineering C*[J], 2004, 24(6): 745

8 Jiang Z, Norby T, Middleton H. *Corrosion Science*[J], 2010, 52(10): 3158

9 Manhabosco T M, Tamborim S M, Santos C B D *et al*. *Corrosion Science*[J], 2011, 53(5): 1786

10 Wang J W, Ma Y, Guan J *et al*. *Surface and Coatings Technology* [J], 2018, 338: 14

11 Narayanan R, Seshadri S K. *Corrosion Science*[J], 2007, 49(2): 542

12 Mantzila A G, Prodromidis M I. *Electrochimica Acta*[J], 2006, 51(17): 3537

13 Xing J H, Xia Z B, Hu J F *et al*. *Corrosion Science*[J], 2013, 75(7): 212

14 Zheng G, Zhang Y, Zhai G X *et al*. *Coal Mine Machinery*[J], 2002, 37(5): 853

15 Zhang L, Duan Y Q, Gao R *et al*. *Materials*[J], 2019, 12(3): 370

16 Capek D, Gigandet M P, Masmoudi M *et al*. *Surface and Coatings Technology*[J], 2008, 202(8): 1379

17 Tong W, Tao N, Wang Z *et al*. *Science*[J], 2003, 299(5607): 686

18 Lei W, Wang Y M, Zhou Y *et al*. *Corrosion Science*[J], 2011, 53(1): 473

19 Ou S F, Wang K K, Hsu Y C. *Applied Surface Science*[J], 2017, 425: 594

20 Gurao N P, Kapoor R, Suwas S. *Acta Materialia*[J], 2011, 59(9): 3431

21 Thomas M, Lindley T, Rugg D *et al*. *Acta Materialia*[J], 2012, 60(13-14): 5040

22 Zhu K Y, Vassel A, Brisset F *et al*. *Acta Materialia*[J], 2004, 52(14): 4101

23 Liu Y, Jin B, Lu J. *Materials Science and Engineering A*[J], 2015, 636: 446

24 Liu Y G, Li M Q, Liu H J. *Materials Characterization*[J], 2016, 123: 83

25 Vesel A, Mozetic M, Drenik A *et al*. *Applied Surface Science*[J], 2008, 255(5): 1759

26 Jiang Z, Dai X, Middleton H. *Materials Science and Engineering B*[J], 2011, 176(1): 79

27 Wang C M, Pan L, Zhang Y A *et al*. *International Journal of Hydrogen Energy*[J], 2016, 41(33): 14 836

28 Si H Y, Sun Z H, Kang X *et al*. *Microporous & Mesoporous Materials*[J], 2009, 119(1-3): 75

29 Ohtsuka T, Guo J, Sato N. *Cheminform*[J], 1987, 18(14): 2473

30 Mccafferty E. *Corrosion Science*[J], 2005, 47(12): 3202

31 Wang Z B, Hu H X, Zheng Y G *et al*. *Corrosion Science*[J], 2016, 103: 50

32 Ou J F, Hu W, Xue M *et al*. *ACS Applied Materials & Interfaces* [J], 2013, 5(8): 3101

33 Fattahalhosseini A. *Arabian Journal of Chemistry*[J], 2016, 9(7): 1342

34 Gannouni M, Assaker I B, Chtourou R. *Materials Research Bulletin*[J], 2015, 61: 519

35 Guo H X, Lu B T, Luo J L. *Electrochimica Acta*[J], 2007, 52(3): 1108

36 Feng Z C, Cheng X Q, Dong C F *et al*. *Corrosion Science*[J], 2010, 52(11): 3646

37 Veluchamy A, Sherwood D, Emmanuel B *et al*. *Journal of Electroanalytical Chemistry*[J], 2017, 785: 196
38 Macdonald D D. *Electrochimica Acta*[J], 2011, 56(4): 1761
39 Fadl-Allah S A, Mohsen Q. *Applied Surface Science*[J], 2010, 256(20): 5849
40 Fernández-Domene R M, Blasco-Tamarit E, García-García D M *et al*. *Electrochimica Acta*[J], 2013, 95: 1
41 Sazou D, Saltidou K, Pagitsas M. *Electrochimica Acta*[J], 2012, 76: 48

表面纳米化对纯钛阳极氧化膜组织及特性的影响

付天琳[1,2]，梅长云[1]，陈飞帆[1]，许志华[1]
(1. 美的集团 生活电器事业部研究院，广东 佛山 528000)
(2. 华南理工大学 材料科学与工程学院，广东 广州 510641)

摘　要：通过表面机械研磨处理（SMAT）制备了表面梯度纳米晶结构，研究了表面纳米化对纯钛阳极氧化膜的表面组织及特性的影响。在30 V恒电位模式、0.5 mol/L H_2SO_4溶液中进行不同时长的阳极氧化处理。使用光学显微镜、X射线衍射、拉曼光谱、光电子能谱及电化学测试研究氧化膜的表面特性及腐蚀抗性。结果表明，梯度纳米晶结构可以增加氧化膜的厚度，促进结晶行为，提高抗腐蚀性。阴阳离子空位凝聚机制能够解释梯度纳米晶结构对抗腐蚀性的影响。

关键词：表面机械研磨处理；梯度纳米晶结构；钛；阳极氧化；陶瓷层；抗腐蚀性

作者简介：付天琳，男，1989年生，博士，美的集团生活电器事业部研究院，广东 佛山 528000，E-mail：futl@midea.com